Full paper/Mémoire

Internal path investigation of the acting electrons during the photocatalysis of panchromatic ruthenium dyes in dye-sensitized solar cells

Nouha Kouki [a], Salma Trabelsi [a], Mohamadou Seydou [b], François Maurel [b], Bahoueddine Tangour [a, *]

[a] Université de Tunis El Manar, Research Unity of Modeling in Fundamental Sciences and Didactics, IPEIEM, BP 254, El Manar 2, 2096, Tunis, Tunisia
[b] Université Paris-Diderot, Sorbonne-Paris-Cité, ITODYS, UMR 7086 CNRS, 15, rue Jean-Antoine-de-Baïf, 75205, Paris cedex 13, France

A R T I C L E   I N F O

A B S T R A C T

A series of heteroleptic Ru(II) complexes were theoretically investigated using time-dependent density functional theory. These dyes, including K8 and N3, are based on a common motif formed by Ru center, N=C=S, and polypyridyl ligands, but differ only by the nature of the added group in *para* position of each pyridyl. The presence of these ligands will enable the evaluation of the electronic effects $\pm$I and $\pm$M. This work focuses on the localization of the part, among the metal, the $-$N=C=S, the polypyridyl ligands, and the added group R, which is most actively involved in the photocatalysis process. We dealt with both ground and excited states as well as the electronic transitions between them. To illustrate the effect of each functional group R on its photophysical properties, the geometries of five dyes were optimized in the molecular and univalent cationic states. All molecules are asymmetrical in shape with a distorted octahedral coordination of the RuN6 core. Atomic charge and spin density distributions show that a charge transfer process occurs from the NCS/Ru to polypyridyl ligand. Analysis of the electronic absorption spectra reveals that the band with the highest wavelength value is assigned to metal-to-ligand charge transfer transition. On the contrary, two other bands are assigned to multi-transitions Ru/NCS to polypyridyl$-\pi^*$. These attributions have been confirmed by the localization of all atoms intervening in them. We also introduced an adapted way to estimate the ionization probability values in each atomic center in the ground and first excited states. Phenomenal properties such as mobility, redox potential, electronic spectrum, ionization potential, and optical gap of the most efficient dye, which is the N3, fit well with experimental values.

© 2018 Académie des sciences. Published by Elsevier Masson SAS. All rights reserved.

1. Introduction

Since the invention of dye-sensitized solar cells (DSSCs) in 1991 [1], these cells are regarded as a cutting-edge technology [2–12] because of their low manufacturing cost and high efficiency [13–24]. Furthermore, these cells are no longer confined to solar panels on the rooftops, because they are invisible, mobile, and foldable [24]. Typically, the "DSSC" converts visible light into electricity via the sensitization of a wide band gap semiconductor using a sensitizing dye steeped in an electrolyte solution, generally the redox couple I^-/I_3^-. Thereby, the photosensitizer constitutes the key element of the cell that performs

* Corresponding author.
  E-mail address: bahoueddine.tangour@ipeiem.utm.tn (B. Tangour).

the double function of light absorption and electron injection into the conduction band (BC) of the semiconductor [25,26].

Up to now, the most successfully used sensitizers in DSSCs are some polypyridyl-ruthenium(II) complexes chemisorbed on mesoporous nanocrystalline TiO_2 films owing to their promising photophysical, electrochemical, and redox properties [26—37]. Although, these sensitizers exhibit a broad range of visible light absorption [13] and long-lived excited state [20], they show a poor red response [38]. The urge to improve the performance of these cells has led to different approaches in modifying the sensitizer's structure to increase the extension of solar absorption spectra from the visible to the near-infrared region. It was found in the literature that using the best anchoring group can upgrade sharply the red shift of the absorption spectra and guaranty a better adsorption of the dye on the TiO_2 film [9].

The sensitizers' molecular structure has a key role in the performance of the DSSC [26]. Our study concerns four chromophores, K8, N3, Dye 1, and Dye 2, relatively to a fifth dye (R = H) considered as reference Dye_{ref} (Fig. 1). They share a main structure of two NCS and two bipyridyl (bpy) ligands around Ru center forming the RuN_6 core. The central atom Ru(II) adopts a low spin electronic configurations $5s^2 4d^6$ in which the six electrons 4d undergo two lone pairs and two single electrons. These two last electrons establish a single bond with each $-N=C=S$ ligand. The remaining vacant 3d and the three 5p orbitals accept the nitrogen lone pair of each bpy group leading to dative bonds as it is indicated in Fig. 1. Therefore, we have an 18-electron complex MX2L4.

Modeling could be used to accelerate the process of developing DSSCs with a substantial saving of time and experimental resources. In this work, we aim to bring a chemist's point of view in the understanding of the functioning mechanism of a cell. This article deals primarily with the dye and in particular with the ionization process.

Our target remains the N3 [12] and K8 [39] cells that differ in nature of the anchoring group. However, if we consider that the good performance of these two cells is, at least in part, because of the anchoring group (which also plays the role of acceptor group because of the attraction of electrons by the electronegative atoms), nothing at best of our knowledge indicates that the electrons injected into TiO_2 pass only through the chemical bonds involving the anchoring group [22,40].

N3 or K8 carry several anchoring groups but only one that is linked to TiO_2 would play the role of assisting electron injection. The others, attracting the electrons, could even play a harmful role. It is for this reason that derivatives of N3 have been developed in which the bpy groups carry other groups. We can cite OC_6H_{13} [41], nC_8H_{17} [42] (Z907), ter-Butyl (Ru) [42], or other bulky patterns [43].

It is in an attempt to study the effects of groups that we have called added groups and not anchoring. Because CH_3 cannot claim this role, we have quoted as a reference a structure without additive groups. For the study to show any effect, it is imperative that the four added groups are similar. CH_3 is donor by effect +I and OCH_3 is donor by effect +M. Our work focused on an analysis of the local properties of the dye in the ground state, excited state, or during the excitation process. We have tried to analyze each electronic effect on the characteristics of the dye to deepen the knowledge of the ionization mechanism. The injection process will be our next goal. The study will then concern dyes comprising several different added groups including anchoring groups.

Studied dyes differ only by nature of the added group noted R. It is equal to $-H$, $-CH_3$, $-OCH_3$, $-COOH$, and $-CH=CH-COOH$ for Dye_{ref}, Dye 1, Dye 2, N3, and K8, respectively (Fig. 1). The selection of this series of dyes was based on the aim that each group introduces a phenomenon assumed to improve the efficiency of the cell. Dye 1 presents an electron donor alkyl group with inductive effect (+I) that may also introduce a steric effect. Dye 2
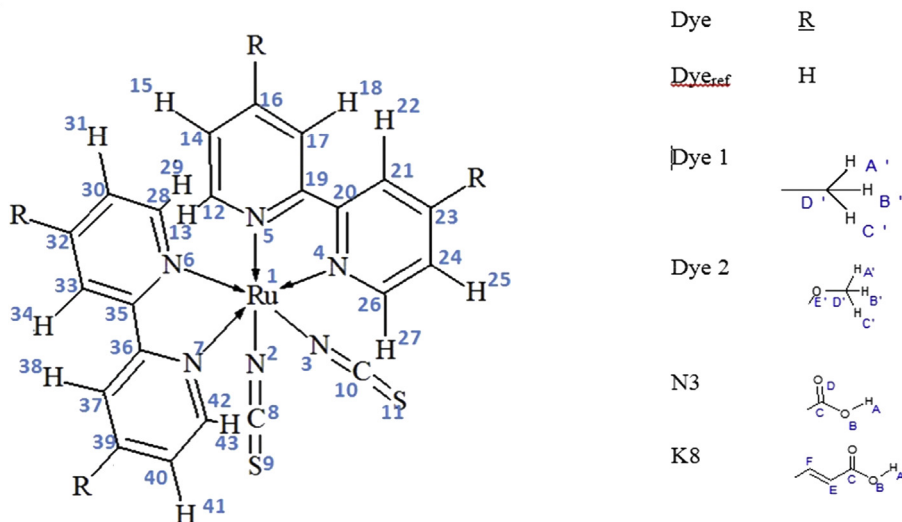

Fig. 1. Labeling of studied molecules.

incorporates an oxygen atom through the methoxy moiety. In this case, the oxygen atom generates not only an inductive effect (−I) but also possibly a donor effect (+M) through its lone pair. The group that is supposed to have the best coupling with TiO$_2$ electrode and so plays the role of an anchoring group is the carboxylic acid group present in dye N3. Finally, the introduction of a conjugated sequence within the carboxylic acid group in the dye K8 is supposed to upgrade the efficiency and the thermal stability of the device [44–47].

To be suitable for DSSCs' applications, dyes must show some intrinsic properties such as (1) a large electronic absorption capacity in the visible region and (2) a preferably donor−acceptor anchoring group directional structure. Thus, the effect of changing the added group was discussed in detail in this study. This will concern properties in both ground and excited states as well as that related to the electronic transition between them. Our main goal was to highlight the relationship between structural or energetic features and intramolecular electronic path associated with the photovoltaic process. This seems to be an important step in the elucidation of the mechanism controlling the efficiency of the cell. We will look for the ability of each dye to undertake an electronic transition or to ionize a particular part of the dye and prioritize the properties at the origin of the photovoltaic phenomenon. To properly locate the electronic distribution in each of these situations, we proceeded to the optimization of the geometry, carried out calculations concerning the atomic probabilities of ionization, the molecular orbitals, and the spectroscopic properties, and then finished by computing certain properties of dyes' work such as mobility, reorganization energy, and redox potential calculations.

2. Computational details

Computations are carried out in the gas phase and ethanol solution. We used the density functional theory (DFT) [48] implanted in the Gaussian (09) program package [49] and time-dependent density functional theory (TD-DFT) [50] extension referred to a B3LYP [51] hybrid functional, at both molecular and the univalent cationic states. Values in ethanol solution were calculated using the polarizable conductor calculation model (CPCM) solvation model [52].

Small core relativistic pseudo-potentials (penta-ζ effective core potentials [ECPs]) were assigned to describe the ruthenium (Ru), and a triple ζ 6-311G* basis set [53] was used including polarization function for all of the other atoms except hydrogen. Hereafter, on the basis of the optimized structures, atomic charges and Wiberg Bond Indexes (WBI) were determined using natural bonding orbitals (NBOs) [54]. Finally, electronic absorption properties were engineered using TD-DFT.

3. Results and discussion

3.1. Ground state

3.1.1. Geometry optimization

It is customary to start a theoretical calculation by the optimization of geometry because it represents an opportunity to validate the choices of the adopted calculation method. In addition, we stated that our main purpose is to describe as fully as possible the electronic path from the photoionization of the dye. Bond length analysis is a powerful tool for describing the distribution of electronic density in terms of bond order and conjugation. In addition, we have extended the analysis to cations created by the ionization process.

The five studied dyes are represented in Fig. 1, in which we have indicated atom labeling of the common part by means of Arabic numbers. We used Latin letters to designate the atoms of the different added groups, which are −H, −CH$_3$, −OCH$_3$, −COOH, and −CH═CH-COOH for Dye$_{ref}$, Dye 1, Dye 2, N3, and K8, respectively. The optimized structures in their ground state have been reported in Fig. 2. All bond length values are gathered in Table 1. It is clear that the theoretical values are consistent with experimental ones, which validates the adopted level of calculation.

All studied molecules are asymmetrical in shape and they exhibit a distorted octahedral coordination geometry for the RuN$_6$ core. Thus, we will be able to specify the role of the common part of these dyes with the role of each added groups. Bearing in mind that the bond lengths are measurable parameters and sensitive to electronic effects, it is worth to scrutinize their variation from molecular to cationic state. This will give us an idea about the roles of each atom in the internal process leading to the departure of the electron. Indeed, an electron that comes out from a chemical bond weakens it leading to an increase in its length. On the contrary, an electron that comes out from a lone pair will have much less effect on the neighboring chemical bonds.

On the other hand, the departure of an electron will generate a positive charge, which will be shared by a certain number of atomic centers because of the presence of several conjugation zones in each molecule. A positive charge increase can lead to the shortening of the chemical bond in which this atom participates.

We begin by stating that by passing from the added group with the largest donor capacity (R: CH$_3$) to that with the largest acceptor capacity (R: −C═C-COOH), the Ru-N bonds are strengthened. The bond lengths of molecular states are close varying from 2.045 to 2.093 Å, which is a low variation of about 2.3%. These values are characteristic of simple Ru-N bonds. They do not exhibit the same behavior during the ionization process.

The two distances Ru-N contracted with the nitrogen atoms of the −N═C═S groups have decreased by 2.7% from 2.045 to 1.991 Å, for example for N3. Conversely, the Ru-N distances of the bpy groups increased by 1.8% from 2.077 to 2.115 Å for N3.

The C-S bonds also increased by 1.3%, which promotes the electron departure from the lone pair of the sulfur for the −N═C═S group and the lone pair of the nitrogen for the bpy ligands.

The variations we have just noticed are significant even if they do not give rise to changes in the bond order. For instance, passing the C-C bond from single to double bond produces a variation of about 14%. It is interesting to note that all of the five studied dyes have the same type of variations as those that we observed with N3.
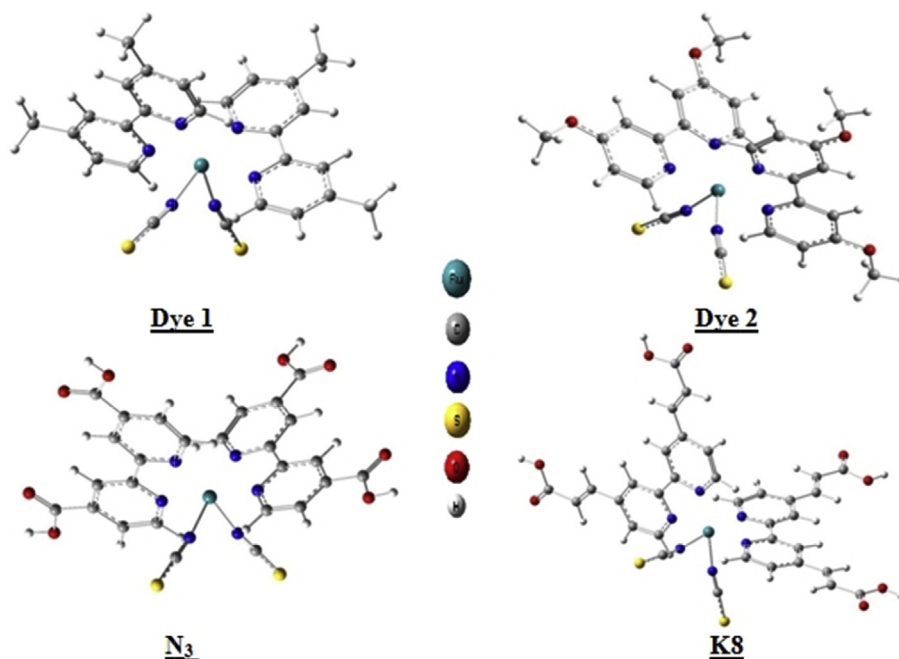
Fig. 2. Optimized structures of the studied dyes in their molecular states.

Table 1
Selected bond lengths of studied dyes in the molecular (M) and univalent cationic (M$^+$) states (expressed in Å).

Bond	Dye$_{ref}$		Dye 1		Dye 2		N3		K8		Experimental [55]
	M	M$^+$	M	M$^+$	M	M$^+$	M	M$^+$	M	M$^+$	M
Ru1-N2	2.053	1.992	2.055	1.994	2.057	1.994	2.045	1.991	2.044	1.993	2.048–2.046
Ru1-N3	2.053	1.992	2.055	1.994	2.057	1.994	2.045	1.991	2.044	1.993	
Ru1-N4	2.083	2.118	2.084	2.115	2.093	2.117	2.077	2.115	2.076	2.114	2.036–2.058
Ru1-N5	2.079	2.098	2.080	2.098	2.086	2.101	2.074	2.098	2.075	2.095	
Ru1-N6	2.083	2.118	2.084	2.115	2.093	2.117	2.077	2.115	2.076	2.114	
Ru1-N7	2.079	2.098	2.080	2.098	2.086	2.101	2.074	2.098	2.075	2.095	
N2-C8	1.177	1.184	1.176	1.184	1.176	1.183	1.178	1.184	1.178	1.184	1.162–1.103
N3-C10	1.177	1.184	1.176	1.184	1.176	1.183	1.178	1.184	1.178	1.840	
C8-S9	1.630	1.607	1.632	1.608	1.634	1.609	1.626	1.606	1.626	1.607	1.615–1.685
C10-S11	1.630	1.607	1.632	1.608	1.634	1.609	1.626	1.606	1.626	1.607	

To better quantify these changes in terms of bond orders, we performed a calculation of the WBIs (Table 2). The K8 complex shows the strongest Ru-N bond indexes with a difference of 11% as compared with the Dye$_{ref}$. The strengthening of these Ru-N bonds is at the expense of N≡C bonds of the thiocyanate to ligands whose WBIs were diminished from 2.3 in Dye$_{ref}$ to 2.1 in K8. The WBIs, however, retain the same order of magnitudes, confirming our previous conclusion in the absence of an explicit change in the bond orders and highlighting the scattering

Table 2
WBIs in molecular (M) and univalent cationic (M$^+$) states.

Bond	Dye$_{ref}$		Dye 1		Dye 2		N3		K8	
	M	M$^+$	M	M$^+$	M	M$^+$	M	M$^+$	M	M+
Ru1-N2 (NCS)	0.64	0.75	0.64	0.71	0.68	0.72	0.66	0.70	0.73	0.70
Ru1-N4 (bpy)	0.57	0.53	0.57	0.58	0.52	0.58	0.59	0.57	0.65	0.57
Ru1-N5 (bpy)	0.56	0.54	0.56	0.57	0.54	0.56	0.57	0.56	0.63	0.55
Ru1-N6 (bpy)	0.57	0.53	0.57	0.58	0.52	0.58	0.59	0.57	0.65	0.57
Ru1-N7 (bpy)	0.56	0.54	0.56	0.57	0.54	0.56	0.57	0.56	0.64	0.55
N2-C8	2.30	2.18	2.31	2.23	2.28	1.64	2.28	2.23	2.09	2.23
C8–S9	1.58	1.70	1.57	1.63	1.59	1.69	1.61	1.65	1.77	1.65

of the atomic centers through which the electrons are ejected, during the ionization.

3.1.2. Atomic charges and spin densities

To get insight in the charge transfer process involved in the photoexcitation of the sensitizers, atomic charge distribution in both molecular and univalent cationic states are computed and reported in Table 3.

Because we have shown the existence of several centers by which the electrons can be ejected, we have indicated the sum of NBO charges per ligand.

The charge distribution unambiguously shows that the Ru atoms have been optimized as positively charged in both molecular and cationic states with atomic charges in the range of 0.31–0.35 with a slight predominance of the cationic state. In contrast, thiocyanate groups were considered to be negatively charged with a significantly increased charge passing to the cationic state. These values are consistent with the intuition of chemists who consider that the ruthenium is in the degree of oxidation +2 and would be twice positively charged with the configuration $5s^0 4d^6$. Similarly, each NCS ligand would be negatively charged. The transition to the cationic state spawns a distribution of the positive charge in several centers. It is clear that each ligand (−NCS, bpy, or added group) has contributed by nearly 1/5, thus confirming the importance of each ligand in the structure of the studied dyes. The atomic charge of the R groups has also risen in the cationic state.

If these results show the distribution of the positive electric charge on several parts of the molecule as a consequence of the conjugation, the distribution of the spin density shows that the remaining single electron is quasi-equally distributed between the Ru center and the −N≡C≡S ligands. Then, at the cationic state, the Ru atoms exhibit a spin density of about 0.50 and that of the thiocyanate moiety is of about 0.50 for Dye 1, Dye 2, and N3 and a value of 0.49 for the dye K8 unlike bpy and R groups, which have almost nil spin densities. The spin density values substantiate our prediction of the charge transfer process.

3.1.3. Ionization probability

In this section, we are interested in the variation of the electrical charge on each atom and not each ligand (Fig. 3). We will transform this variation to an estimation of the ionization probability (IPr) of each atom of the dye with the aim to locate the "exit gates" of the electrons and to compare the ability of the dyes in the injection of electrons into the semiconductor oxide BC.

To compute the atomic IPr values (Table 4), the Eq. 1 was used:

$$IPr(\%) = (NBO\ charge\ of\ M^+ - NBO\ charge\ of\ M) * 100 \quad (1)$$

The correlation between the different functional groups and the reference unambiguously shows that the addition of the Me group does not seem to be decisive because it does not cause significant changes in the IPr as compared to the reference.

3.2. Description of electronic transitions

3.2.1. Molecular frontier orbitals

To further understand the charge transfer process, there is a quest to have a look at the molecular frontier orbitals. Experimental determination of their energies is extracted from ultraviolet photoelectronic spectroscopy. Highest occupied molecular orbital (HOMO) and lowest unoccupied molecular orbital (LUMO) energy values of the dye N3 [56] are equal to −5.47 and −3.93 eV, respectively. The corresponding optical gap is about 1.54 eV. Our corresponding calculated values (Table 5) for N3 are equal to −5.035, −3.413, and 1.622 eV. We can conclude that our calculation method describes correctly the energetic behavior of N3 and that our predictive values for the other dyes are reliable.

Indeed, our study has revealed that HOMO and HOMO − 1 of the four sensitizers (Dye 1, Dye 2, N3, and K8) are localized on the Ru atom and the NCS ligands. However, LUMO and LUMO + 1 are located evenly on the two bpy ligands. This distribution confirms that the thiocyanate groups (NCS) and the metal center are donor groups, whereas the bpy ligands are acceptor ones (Figs. 4 and 5). Because bpy groups come into contact with TiO_2 by means of the anchoring groups, this result favored the electron injection into the TiO_2 BC. This outcome has been well confirmed in the literature [57].

From an energy standpoint, the orbital levels are minimally affected for molecules having electronegative groups (Dye 2, N3, and K8), unlike the Dye 1 that shows a higher value of the LUMO, which indicates that the methyl group is less good acceptor than other groups. The small variation in the LUMO energies between N3 and K8 (= 0.006 eV) shows that adding the C≡C bond has no big influence on this parameter.

Reverting to the DSSC, by comparing the LUMO positions to the TiO_2 BC levels, we can conclude that our four chromophores are capable of injecting, in the excited state,

Table 3
NBO atomic charge (Q) and spin densities (S) of the dyes in molecular (M) and univalent cationic (M^+) states.

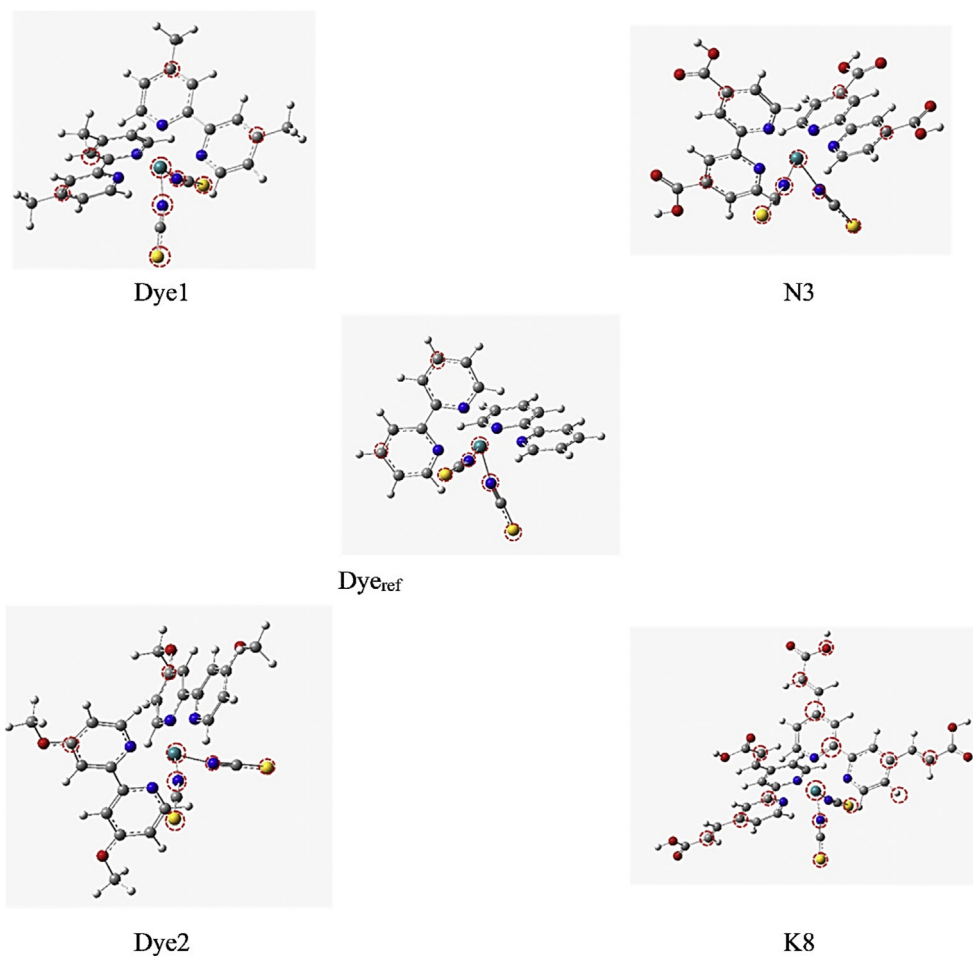| Bond	Dye_ref		Dye 1			Dye 2			N3			K8		
	M	M^+		M	M^+		M	M^+		M	M^+		M	M^+
	Q	Q	S	Q	Q	S	Q	Q	S	Q	Q	S	Q	Q	S
Ru1	0.33	0.43	0.51	0.33	0.42	0.45	0.32	0.41	0.50	0.35	0.36	0.47	0.31	0.37	0.51
NCS	−0.60	−0.33	0.49	−0.60	−0.34	0.55	−0.59	−0.34	0.50	−0.56	−0.28	0.47	−0.49	−0.31	0.49
Bpy	−0.04	0.08	0.00	0.11	0.20	0.00	0.27	0.36	0.01	0.09	0.25	0.07	0.20	0.32	−0.01
2R	0.42	0.45	0.01	0.11	0.16	0.00	−0.39	−0.33	0.00	0.07	0.12	0.00	0.02	0.14	0.00

Dye1

N3

Dye_ref

Dye2

K8

Fig. 3. Designation of atoms exhibiting IPr values greater than 5% for the studied dyes in their ground state.

Table 4
The calculated IPr values (>10%) for the five dyes.

Dye_ref	IPr	Dye 1	IPr	Dye 2	IPr	N3	IPr	K8	IPr
Ru1	14	Ru1	10	Ru1	12	Ru1	10	Ru1	10
S10	33	S10	29	S10	32	S10	30	S10	23
S11	33	S11	29	S11	32	S11	30	S11	21

an electron in the BC of this semiconductor. The lowest HOMO−LUMO gap of 1.419 eV is assigned to the dye K8, which is beneficial for the charge separation process in the DSSC.

3.2.2. Electronic spectroscopy

There is a quest to explore the absorption spectra of the photosensitizers to allow optical characterization of the sensitizers in the UV−visible region. The electronic absorption of the five dyes in the gas phase was engineered using the TD-DFT method with the hybrid B3LYP functional. The calculated wavelengths (λ), the transition energies, and the oscillator strengths (f) of the molecular orbital were organized according to their energies in Table 5.

The absorption spectra of all chromophores (Fig. 6) properly show the presence of three bands labeled I, II, and

Table 5
Electronic absorption of the studied dyes.

Dye	λ(nm)	Energy (eV)	f	Attribution
N3	373	3.32	0.1510	H-5 → L + 3 (+55%)
				H-4 → L + 2 (+36%)
	446	2.78	0.186	H-6 → L + 0 (+70%)
				H-5 → L + 1 (+21%)
	670	1.85	0.06	H-0 → L + 3 (+55%)
K8	365.5	3.39	0.0807	H-5 → L + 2 (+86%)
	416	2.98	0.1008	H-6 → L + 0 (+67%)
	611	2.03	0.1595	H-2 → L + 3 (+43%)
	612	2.02	0.1506	H-2 → L + 4 (+43%)
				H-3 → L + 3 (+22%)
Dye 1	328	3.77	0.0296	H-6 → L + 2 (+73%)
	426	2.91	0.1181	H-6 → L + 0 (+75%)
	742	1.67	0.0265	H-2 → L + 3 (+43%)
Dye 2	346	3.59	0.0288	H-6 → L + 2 (+72%)
	441	2.81	0.1039	H-6 → L + 0 (+48%)
				H-5 → L + 0 (+20%)
	659	1.88	0.0233	H-3 → L + 1 (+98%)

III. The bands I and II, centered respectively at 300 and 400 nm, are assigned to multitransitions Ru/NCS to polypyridyl−π^* on behalf of the Ru/NCS t_{2g}−π^* and t_{2g}−π orbitals. The wideband III ranging from 600 to 700 nm is
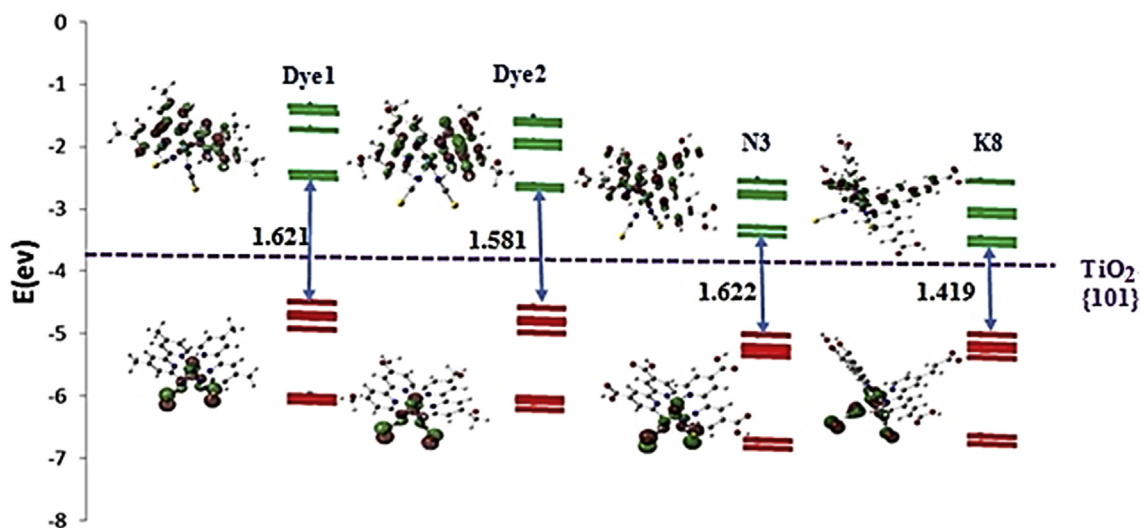
Fig. 4. Energy and representation of the molecular orbitals of the studied dyes (HOMO-6 → HOMO (red) and LUMO → LUMO + 4 (green)), HOMO–LUMO gaps, and the position of the BC of the TiO$_2$.

attributed to metal-to-ligand charge transfer (MLCT) transition. For the dye N3, we can compare our obtained values to experimental ones [58] that are about 538, 398, and 314 nm.

Theoretical values are higher of about 10–20% than experimental ones measured in ethanol. Other theoretical calculations [59,60] also give overestimated absorbed wavelengths in the gas phase but more accurate values in ethanol. The UV–visible absorption spectrum shows that band III of dye N3 exhibits a hypochromic shift as compared with dye K8 because of the absence of the CH=CH group. Furthermore, a hypsochromic shift of the band I of the Dye 1 and the Dye 2 is observed, resulting from the donor effect of their adding groups. Wavelengths were organized according to their energies in the Table 5.

3.3. First excited state

We used a similar process to estimate the atomic IPr for the excited state. In Fig. 7, the most ionized sites in the five excited states of dyes were circled. They correspond to atoms exhibiting IPr values greater than 5% for the studied dyes in their ground state. They are mainly on the metal, the sulfur, the added groups, and the carrier carbons.

It is important to indicate that the atoms of anchoring groups of N3 and K8 participate in the photoionization process. It is the efficient electronic transition of MLCT type, which has enabled this participation.

3.4. Usual descriptors

3.4.1. Ionization potential and electronic affinity

The ionization potential (IP) and electronic affinity (EA) are important factors for the rational design of photovoltaic cells. They can be calculated using the following equations. Adiabatic values are shown in Table 6.

$$IP = E(M^+) - E(M)$$

$$EA = E(M) - E(M^-)$$

The insertion of a conjugated sequence within the carboxylic acid group in the dye K8 has led to a decrease in the value of IP and an increase in the EA value (as compared with dye N3), which means that the hole forming ability and the tendency to add electrons are enhanced.

3.4.2. Mobility

The reorganization energy λ is the required energy associated with the relaxation of the molecular structure after the occurrence of electron transfer. Intramolecular transfer of a hole or an electron can be represented by the Eq. 2 in which M and $M^{+/-}$ designate the molecule in its ground state and the cationic or anionic species, respectively:

$$M^{+/-} + M \rightarrow M + M^{+/-} \tag{2}$$

The corresponding Jablonski diagram is represented in Fig. 8. The reorganization energy of the holes' transport λ_{hole} is given by $\lambda_1 + \lambda_2$. Similar one relatively to the electron is noted $\lambda_{electron}$ and calculated as the sum $\lambda_3 + \lambda_4$. The transfer reorganization energy, which is inversely proportional to the mobility of charge carriers [61] of the hole and the electron, is defined by Eqs 3 and 4:

$$\lambda_{hole} = \lambda_1 + \lambda_2 = [E^0(M^+) - E^0(M)] + [E^1(M) - E^1(M^+)] \tag{3}$$

$$\lambda_{electron} = \lambda_3 + \lambda_4 = [E^0(M^-) - E^0(M)] + [E^1(M) - E^1(M^-)] \tag{4}$$

$E^0(M)$ and $E^1(M^{+/-})$ represent the energy of the molecule or the ion in its ground state but $E^1(M)$ and $E^0(M^{+/-})$

	HOMO−1	HOMO	LUMO	LUMO+1

Dye1

E= -4.708 eV　　E= -4.483 eV　　E= -2.527 eV　　E= -2.466 eV

Dye2

E= -5.217 eV　　E= -5.035 eV　　E= -3.414 eV　　E= -3.298 eV

N3

E= -5.217 eV　　E= -5.035 eV　　E= -3.413 eV　　E= -3.299 eV

K8

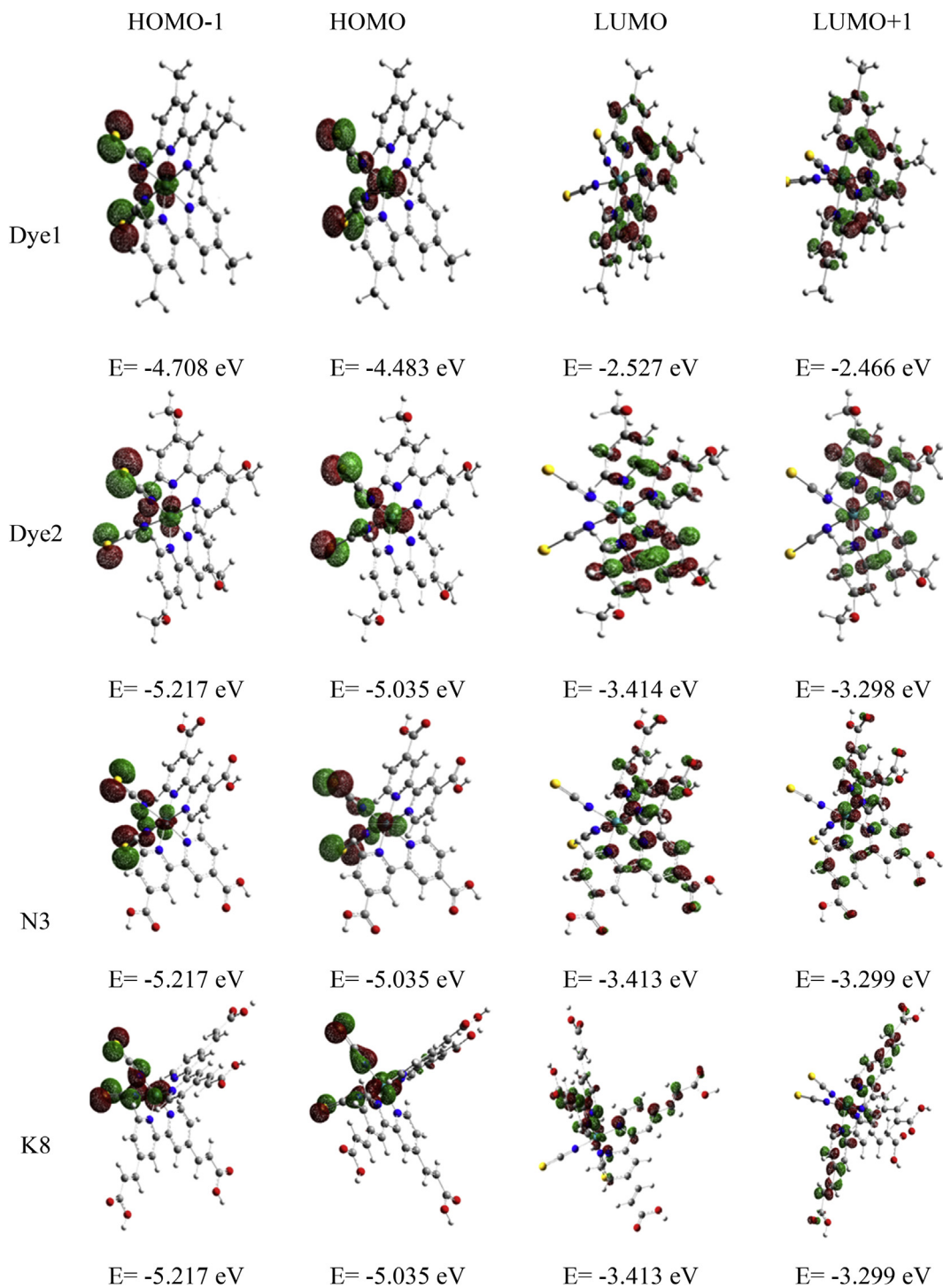E= -5.217 eV　　E= -5.035 eV　　E= -3.413 eV　　E= -3.299 eV

Fig. 5. Selected molecular orbitals and energies of the dyes.

are the energies of M in the optimized geometry of the ion and the energy of the ion in the optimized geometry of the neutral molecule.

The charge transport rate could be approximated by the Marcus electron transfer theory [62,63] given by the Eq. 5:

$$K = \frac{4\pi^2}{h} \frac{1}{\sqrt{4\pi\lambda k_B T}} V^2 \exp\left(-\frac{\lambda}{4\pi k_B T}\right) \qquad (5)$$

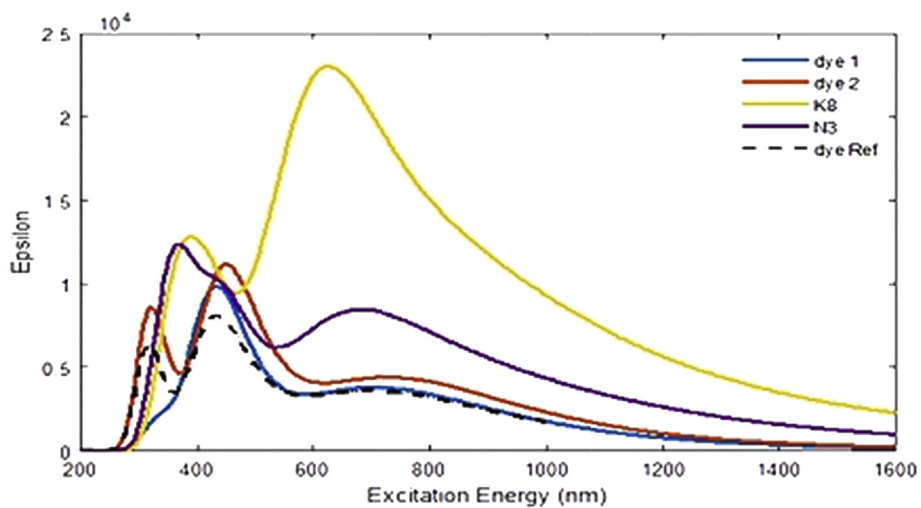where h is the Planck constant, k_B is the Boltzmann constant, T is the temperature, λ is the reorganization energy

Fig. 6. Calculated absorption spectra of the studied dyes.
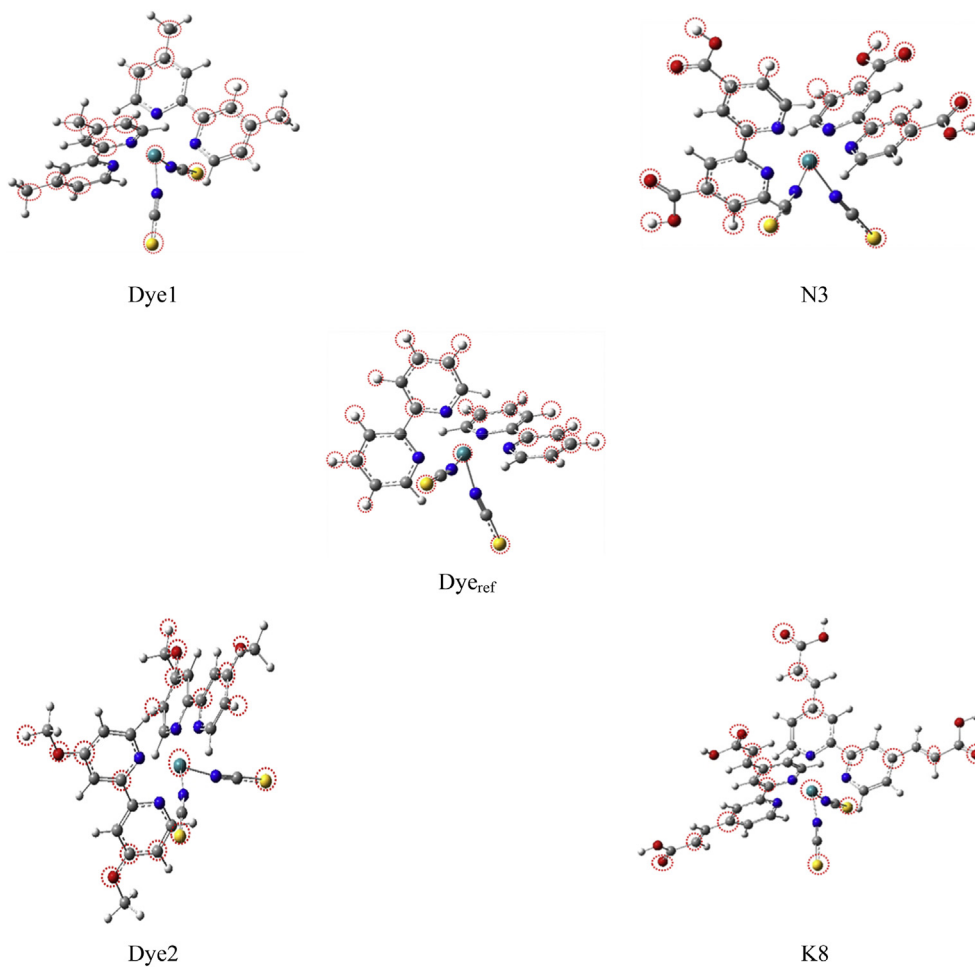

Dye1

N3

Dye$_{ref}$

Dye2

K8

Fig. 7. Designation of atoms exhibiting IPr values greater than 5% for the studied dyes in their excited state.

Table 6
Ionization potential and electronic affinity.

Dye	IP (eV)	EA (eV)
Dye 1	5.49	1.57
Dye 2	5.26	1.36
N3	6.03	2.50
K8	5.93	2.76

Table 7
Reorganization energy values (in eV) calculated for the hole and the electron.

Dye	$\lambda 1$	$\lambda 2$	$\lambda 3$	$\lambda 4$	λ_{hole}	$\lambda_{electron}$	λ_{total}
Dye 1	0.118	0.113	0.006	0.175	0.231	0.181	0.412
Dye 2	0.141	0.134	0.008	0.212	0.275	0.220	0.495
N3	0.126	0.114	0.165	0.160	0.241	0.325	0.565
K8	0.115	0.105	0.125	0.135	0.220	0.260	0.480

for hole or electron, and V is the intermolecular electronic transfer integral between neighboring molecules.

Therefore, the transport process is determined by two important molecular parameters: the internal reorganization energy (λ), which must be low for efficient charge transport, and the integral of the intermolecular hole or electron (V) that describes the electronic force coupling between neighboring molecules. The former requires a tight crystal package and good intermolecular pairing between the boundary molecular orbitals, whereas the latter favors long, planned, and conjugated molecules, with less flexible degrees of freedom. Our calculated values are gathered in Table 7.

Experimental [64] reorganization energy value for N3 is equal to 0.554 eV. Our calculated value is equal to 0.565 eV, which is very close to the experimental one. Except for dye K8, the values of λ_{hole} are greater than $\lambda_{electron}$ for all of the dyes, which indicates a better electron transport performance because λ is inversely proportional to the mobility of charge carriers. By comparing Dye 1 and Dye 2, the methyl group (Dye 1) substitution by a methoxy (Dye 2) leads to an increase in both λ_{hole} and $\lambda_{electron}$ and so improves the charge mobilities. Comparing the N3 and K8 dyes, we can deduce that the addition of the conjugation at the anchoring group disadvantages the carrier's mobility.

3.4.3. Redox potential
To find the redox potential, a method related to the thermodynamics was used according to the Scheme 1:

$$\Delta_r G^{\circ}_{(solv)} = \Delta_r G^{\circ}_{(g)} - \Delta G^{\circ}_{(solv)}(M) - \Delta G^{\circ}_{(solv)}(H^+)$$
$$+ \Delta G^{\circ}_{(solv)}(M^+) + \frac{1}{2}\Delta G^{\circ}_{(solv)}(H_2) \qquad (6)$$

Hereafter, the redox potential E^0 can be calculated via relation (7):

$$\Delta_r G^{\circ}_{(solv)} = -nFE^0 \qquad (7)$$

where $n = 1$ and F represents the Faraday constant ($F = 96{,}485$ C/mol). $\Delta G^{\circ}_{(solv)}$ was calculated by means of relation (6) using the CPCM model on the Gaussian 09 code in a solution of ethanol.

E^0 values of dyes N3, K8, Dye 1, and Dye 2 are depicted in Table 8 and lie in the range from 0.30 to 0.78 V. Correlation between the calculated value of the redox potential (E^0) of N3 (0.78 V) and the available experimental value (0.85 V) [65,66] shows to be in good agreement. N3 and K8 exhibit the highest values. This is attributed to electron-withdrawing properties of carboxylate groups.

4. Conclusions

In this work, we studied in detail the electronic, geometrical, and spectroscopic properties of five
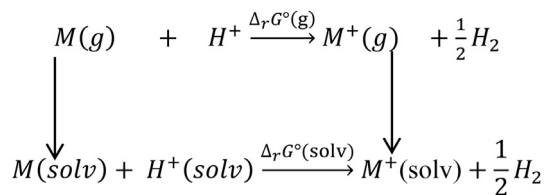
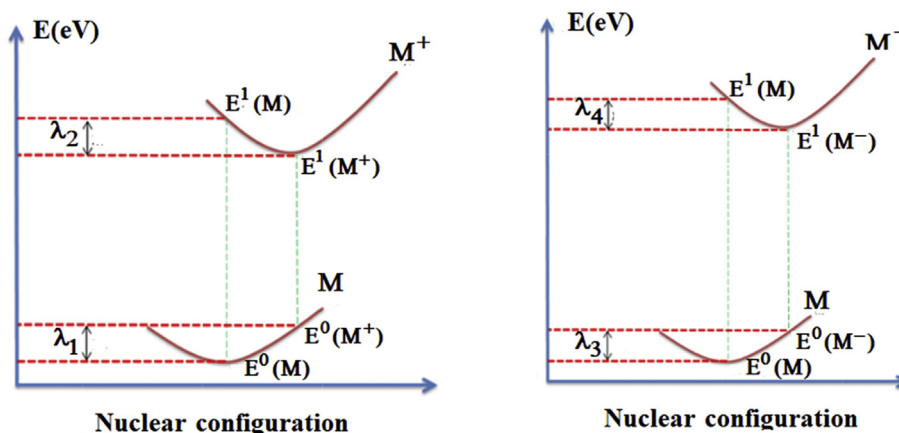**Scheme 1.** The reaction adopted for the calculation of redox potentials.

Fig. 8. Jablonski diagram of the intermolecular transfer reaction between neutral molecule and cationic/anionic specie.

Table 8
Calculated redox potentials (^{E0}) of the five studied dyes $\Delta_r G°$ and ^{E0} (expressed in kJ mol^{-1} and V).

Dye	$\Delta_r G°$(solv)	E^0_{theo}	E^0_{exp}
N3	−74.988	0.78	0.85[a]
K8	−62.686	0.65	
Dye1	−41.365	0.43	
Dye2	−28.638	0.30	

[a] Experimental data from Refs. [65,66].

sensitizers derived from dye N3 in the gas phase by means of combined DFT and TD-DFT functional. Calculated atomic charge, spin densities, and molecular orbitals reveal that the charge transfer occurs from the excited electron of the NCS/Ru to polypyridyl ligand. Analysis of the electronic absorption spectra shows that the band with the highest wavelength value is assigned to MLCT transition contrary to the other two bands, which are assigned to multitransitions Ru/NCS to polypyridyl−π*. The estimation of the IPr values reveals that the most efficient process enables atoms of added groups to participate in photoionization because the charge distribution is steered to the bpy ligands.

References

[1] B. O'Regan, M. Grätzel, Nature 353 (1991) 737−740.
[2] T. Le Bahers, F. Labat, T. Pauporté, P.P. Lainé, I. Ciofini, J. Am. Chem. Soc. 133 (2011) 8005−8013.
[3] C.-Y. Li, C. Su, H.-H. Wang, P. Kumaresan, C.-H. Hsu, I.-T. Lee, W.-C. Chang, Y.S. Tingare, T.-Y. Li, C.-F. Lin, W.-R. Li, Dyes Pigm. 100 (2014) 57−65.
[4] Y. Pellegrin, L. Le Pleux, E. Blart, A. Renaud, B. Chavillon, N. Szuwarski, M. Boujtita, L. Cario, S. Jobic, D. Jacquemin, F. Odobel, J. Photochem. Photobiol. Chem. 219 (2011) 235−242.
[5] J.W. Ondersma, T.W. Hamann, Coord. Chem. Rev. 257 (2013) 1533−1543.
[6] P. Rajakumar, V. Kalpana, S. Ganesan, P. Maruthamuthu, Tetrahedron Lett. 52 (2011) 5812−5816.
[7] S. Kämper, A. Paretzki, J. Fiedler, S. Záliš, W. Kaim, Inorg. Chem. 51 (2012) 2097−2104.
[8] H. Li, Z. Xie, Y. Zhang, J. Wang, Thin Solid Films 518 (2010) e68−e71.
[9] F. Angelis, S. Fantacci, A. Selloni, M.K. Nazeeruddin, M. Grätzel, J. Am. Chem. Soc. 129 (2007) 14156−14157.
[10] M.-X. Li, X. Zhou, B.-H. Xia, H.-X. Zhang, Q.-J. Pan, T. Liu, H.-G. Fu, C.-C. Sun, Inorg. Chem. 47 (2008) 2312−2324.
[11] E. Tamburri, V. Guglielmotti, S. Orlanducci, M.L. Terranova, Inorg. Chim. Acta 377 (2011) 170−176.
[12] J. Gong, J. Liang, K. Sumathy, Renew. Sustain. Energy Rev. 16 (2012) 5848−5860.
[13] Q.-J. Pan, Y.-R. Guo, L. Li, S.O. Odoh, H.-G. Fu, H.-X. Zhang, Phys. Chem. Chem. Phys. 13 (2011) 14481−14489.
[14] G. Li, L. Ray, E.N. Glass, K. Kovnir, A. Khoroshutin, S.I. Gorelsky, M. Shatruk, Inorg. Chem. 51 (2012) 1614−1624.
[15] S. Noureen, R. Argazzi, A. Monari, M. Beley, X. Assfeld, C.A. Bignozzi, S. Caramori, P.C. Gros, Dyes Pigm. 101 (2014) 318−328.
[16] Y. Lee, J. Chae, M. Kang, J. Ind. Eng. Chem. 16 (2010) 609−614.
[17] F.-L. Chen, A. Letortu, C.-Y. Liao, C.-K. Tsai, H.-L. Huang, I.-W. Sun, Y.-L. Wei, H. Paul Wang, Nucl. Instrum. Methods Phys. Res. Sect. A 619 (2010) 112−114.
[18] P. Ekanayake, M.R.R. Kooh, N.T.R.N. Kumara, A. Lim, M.I. Petra, V.N. Yoong, L.C. Ming, Chem. Phys. Lett. 585 (2013) 121−127.
[19] G.C. Vougioukalakis, A.I. Philippopoulos, T. Stergiopoulos, P. Falaras, Coord. Chem. Rev. 255 (2011) 2602−2621.
[20] J. Wang, S. Cong, S. Wen, L. Yan, Z. Su, J. Phys. Chem. C 117 (2013) 2245−2251.
[21] M.K. Nazeeruddin, E. Baranoff, M. Grätzel, Sol. Energy 85 (2011) 1172−1178.
[22] J. Gong, K. Sumathy, Q. Qiao, Z. Zhou, Renew. Sustain. Energy Rev. 68 (2017) 234−246.

[23] F. Gao, Y. Wang, D. Shi, J. Zhang, M. Wang, X. Jing, R. Humphry-Baker, P. Wang, S.M. Zakeeruddin, M. Grätzel, J. Am. Chem. Soc. 130 (2008) 10720−10728.
[24] M.-E. Yeoh, K.-Y. Chan, Int. J. Energy Res. 41 (2017) 2446−2467.
[25] R.S. Shelke, S.B. Thombre, S.R. Patrikar, Int. J. Res. Sci. Adv. Technol. 3 (2013) 131−136.
[26] R.S. Shelke, S.B. Thombre, S.R. Patrikar, Int. J. Renew. Energy Resour. 3 (2013) 54−61.
[27] S. Lu, R. Geng, T. Wu, B. Ren, Synth. Met. 170 (2013) 19−24.
[28] R. Srivastava, Comput. Theor. Chem. 1045 (2014) 47−56.
[29] H.-J. Park, K.H. Kim, S.Y. Choi, H.-M. Kim, W.I. Lee, Y.K. Kang, Y.K. Chung, Inorg. Chem. 49 (2010) 7340−7352.
[30] J. Chen, F.-Q. Bai, J. Wang, L. Hao, Z.-F. Xie, Q.-J. Pan, H.-X. Zhang, Dyes Pigm. 94 (2012) 459−468.
[31] S. Altobello, R. Argazzi, S. Caramori, C. Contado, S. Da Fré, P. Rubino, C. Choné, G. Larramona, C.A. Bignozzi, J. Am. Chem. Soc. 127 (2005) 15342−15343.
[32] K.-Y. Liu, C.-L. Hsu, J.-S. Ni, K.-C. Ho, K.-F. Lin, J. Colloid Interface Sci. 372 (2012) 73−79.
[33] B.-wook Park, L. Yang, E.M.J. Johansson, N. Vlachopoulos, A. Chams, C. Perruchot, M. Jouini, G. Boschloo, A. Hagfeldt, J. Phys. Chem. C 117 (2013) 22484−22491.
[34] K. Ocakoglu, S. Sogut, H. Sarica, P. Guloglu, S. Erten-Ela, Synth. Met. 174 (2013) 24−32.
[35] K. Srinivas, K. Yesudas, K. Bhanuprakash, V.J. Rao, L. Giribabu, J. Phys. Chem. C 113 (2009) 20117−20126.
[36] F.-T. Kong, S.-Y. Dai, K.-J. Wang, Adv. Optoelectron. 2007 (2007) 1−13.
[37] A. Hinsch, W. Veurman, H. Brandt, K.F. Jensen, S. Mastroianni, ChemPhysChem 15 (2014) 1076−1087.
[38] M. Aliaghayee, H. Ghafoori Fard, A. Zandi, J. Porous Mater. 22 (2015) 1617−1626.
[39] T.M.W.J. Bandara, H.D.N.S. Fernando, E.J. Rupasinghe, J.L. Ratnasekera, P.H.N.J. Chandrasena, M. Furlani, I. Albinsson, M.A.K.L. Dissanayake, B.E. Mellander, Ceylon J. Sci. 45 (2016) 61.
[40] G. Benkö, J. Kallioinen, J.E.I. Korppi-Tommola, A.P. Yartsev, V. Sundström, J. Am. Chem. Soc. 124 (2002) 489−493.
[41] S. Mathew, A. Yella, P. Gao, R. Humphry-Baker, B.F.E. Curchod, N. Ashari-Astani, I. Tavernelli, U. Rothlisberger, M.K. Nazeeruddin, M. Grätzel, Nat. Chem. 6 (2014) 242−247.
[42] L. Zedler, F. Theil, A. Csáki, W. Fritzsche, S. Rau, M. Schmitt, J. Popp, B. Dietzek, RSC Adv. 2 (2012) 4463.
[43] H.M. Nguyen, D.N. Nguyen, N. Kim, Adv. Nat. Sci. Nanosci. Nanotechnol. 1 (2010) 25001.
[44] S.B. Akula, H.-S. Chen, C. Su, B.-R. Chen, J.-J. Chiou, C.-H. Shieh, Y.-F. Lin, W.-R. Li, Inorg. Chem. 56 (2017) 12987−12995.
[45] Y. Cao, Y. Bai, Q. Yu, Y. Cheng, S. Liu, D. Shi, F. Gao, P. Wang, J. Phys. Chem. C 113 (2009) 6290−6297.
[46] P. Wang, S.M. Zakeeruddin, J.E. Moser, R. Humphry-Baker, P. Comte, V. Aranyos Anders Hagfeldt, M.K. Nazeeruddin, M. Grätzel, Adv. Mater. (Weinheim, Ger.) 16 (2004) 1806−1811.
[47] Q. Yu, S. Liu, M. Zhang, N. Cai, Y. Wang, P. Wang, J. Phys. Chem. C 113 (2009) 14559−14566.
[48] P. Hohenberg, W. Kohn, Phys. Rev. 136 (1964) B864−B871.
[49] M.J. Frisch, G.W. Trucks, H.B. Schlegel, G.E. Scuseria, M.A. Robb, J.R. Cheeseman, G. Scalmani, V. Barone, G.A. Petersson, H. Nakatsuji, X. Li, M. Caricato, A. Marenich, J. Bloino, B.G. Janesko, R. Gomperts, B. Mennucci, H.P. Hratchian, J.V. Ortiz, A.F. Izmaylov, J.L. Sonnenberg, D. Williams-Young, F. Ding, F. Lipparini, F. Egidi, J. Goings, B. Peng, A. Petrone, T. Henderson, D. Ranasinghe, V.G. Zakrzewski, J. Gao, N. Rega, G. Zheng, W. Liang, M. Hada, M. Ehara, K. Toyota, R. Fukuda, J. Hasegawa, M. Ishida, T. Nakajima, Y. Honda, O. Kitao, H. Nakai, T. Vreven, K. Throssell, J.A. Montgomery Jr., J.E. Peralta, F. Ogliaro, M. Bearpark, J.J. Heyd, E. Brothers, K.N. Kudin, V.N. Staroverov, T. Keith, R. Kobayashi, J. Normand, K. Raghavachari, A. Rendell, J.C. Burant, S.S. Iyengar, J. Tomasi, M. Cossi, J.M. Millam, M. Klene, C. Adamo, R. Cammi, J.W. Ochterski, R.L. Martin, K. Morokuma, O. Farkas, J.B. Foresman, D.J. Fox, Gaussian 09, Revision A.02, Gaussian, Inc., Wallingford CT, 2016. Gaussian 09.
[50] R.F. Nalewajski (Ed.), Density Functional Theory, Springer, Berlin, Heidelberg, New York, 1996 (Topics in Current Chemistry).
[51] D.P. Chong (Ed.), Recent Advances in Density Functional Methods. Singapore, World Scientific, River Edge, NJ, 1995 (Recent advances in computational chemistry).
[52] D.G. Fedorov, K. Kitaura, H. Li, J.H. Jensen, M.S. Gordon, J. Comput. Chem. 27 (2006) 976−985.
[53] R. Ditchfield, W.J. Hehre, J.A. Pople, J. Chem. Phys. 54 (1971) 724−728.

[54] J.P. Foster, F. Weinhold, J. Am. Chem. Soc. 102 (1980) 7211—7218.
[55] V. Shklover, Y.E. Ovchinnikov, L.S. Braginsky, S.M. Zakeeruddin, M. Grätzel, Chem. Mater. 10 (1998) 2533—2541.
[56] J.H. Snook, L.A. Samuelson, J. Kumar, Y.-G. Kim, J.E. Whitten, Org. Electron. 6 (2005) 55—64.
[57] M.K. Nazeeruddin, F. De Angelis, S. Fantacci, A. Selloni, V. Guido, L. Paul, S. Ito, B. Takeru, M. Grätzel, J. Am. Chem. Soc. 127 (2005) 16835—16847.
[58] V. Shklover, M.K. Nazeeruddin, S.M. Zakeeruddin, C. Barbé, A. Kay, T. Haibach, W. Steurer, R. Hermann, H.-U. Nissen, M. Grätzel, Chem. Mater. 9 (1997) 430—439.
[59] G.V. Baryshnikov, B.F. Minaev, V.A. Minaeva, Optic Spectrosc. 110 (2011) 393—400.
[60] C.D.D. Sundari, M.A. Martoprawiro, A.L. Ivansyah, J. Phys. Conf. Ser. 812 (2017) 12068.
[61] I. Kang, H.-J. Yun, D.S. Chung, S.-K. Kwon, Y.-H. Kim, J. Am. Chem. Soc. 135 (2013) 14896—14899.

[62] Z. Shuai, L. Wang, C. Song (Eds.), Theory of Charge Transport in Carbon Electronic Materials, Springer, Berlin, Heidelberg, 2012 (SpringerBriefs in Molecular Science).
[63] Z. Shuai, L. Wang, C. Song, Hopping Mechanism, in: Z. Shuai, L. Wang, C. Song (Eds.), Theory of Charge Transport in Carbon Electronic Materials, Springer, Berlin, Heidelberg, 2012, pp. 7—41. SpringerBriefs in Molecular Science.
[64] F. Manke, J.M. Frost, V. Vaissier, J. Nelson, P.R.F. Barnes, Phys. Chem. Chem. Phys. 17 (2015) 7345—7354.
[65] M.K. Nazeeruddin, A. Kay, I. Rodicio, R. Humphry-Baker, E. Mueller, P. Liska, N. Vlachopoulos, M. Grätzel, J. Am. Chem. Soc. 115 (1993) 6382—6390.
[66] C. Barolo, M.K. Nazeeruddin, S. Fantacci, D. Di Censo, P. Comte, P. Liska, G. Viscardi, P. Quagliotto, F. De Angelis, S. Ito, M. Grätzel, Inorg. Chem. 45 (2006) 4642—4653.